



2025 Science Activities Report



Contents

Executive Summary	3
Introduction	3
Operational User Programme.....	4
Science events.....	6
Grants Activities.....	12
Scientific Publications	14
ESS 2025 – Highlights.....	20

About the cover: The ESS Road to Science is paved with good samples. For NMX, the Neutron Macromolecular Crystallography instrument, this means preparing protein crystals well in advance of neutrons being produced. With the sample preparation area now operational, crystal growth is underway.

These crystals, produced from purified proteins, must be nurtured carefully over many months. It can take between six to 18 months for a single crystal to be ready to be mounted onto the sample stage for experiments. Beginning this work in 2025, with in-house teams and collaborators at partner institutes, ensures that NMX will have the right samples in time for commissioning tests, before welcoming external researchers in 2028.

EXECUTIVE SUMMARY

This report presents an overview of the science activities in 2025 recorded by the Research Coordination Office (RCO). At the close of 2025:

- DEMAX accepted 19 proposals during 2025
- 227 investigators from 15 countries have been on DEMAX proposals since 2019
- 25 science seminars
- 9 science events hosted by the Science Directorate, including ICNS 2025
- ESS has been involved in 69 proposals submitted to several research funders
- ESS is actively taking part in 24 ongoing external grants
- 94 publications that were reported to the library (Scopus)
- 74% were published with some form of Open Access
- H-index all-time is 72
- The publication with the most lifetime citations has been cited 848 times according to Scopus
- The publication from 2025 with the most citations has been cited 12 times
- The total number of citations for ESS during 2025 was 3224
- The total number of citations all time is 26115
- The average number of citations per publication is 18
- ESS averaged 8 citations a day during 2025

INTRODUCTION

The Scientific Activity Report comprises five core elements: an analysis of users served through the call for proposals for the Deuteration and Macromolecular Crystallography (DEMAX) platform, an overview of science events, a review of grant activities, an assessment of ESS's published scientific output in 2025, and a selection of one science highlight per month from the year.

The publication KPIs reported in this document have been collected from Scopus and SciVal. Where needed, manual curation has been made by the library staff. The user KPIs have been extracted from the User Office Software.

OPERATIONAL USER PROGRAMME

Proposals Received

The Deuteration and Macromolecular Crystallisation facility (DEMAX) operated three calls for proposals in 2025, with the final rolling call for proposals open until the 30th January 2026. This report includes all 19 proposals accepted between 1 January and 31 December. Proposals were for chemical deuteration and biological deuteration, with one biological sample requesting subsequent crystallisation.

The publication KPIs reported in this document have been collected from Scopus and SciVal. Where needed, manual curation has been made by the library staff. The user KPIs have been extracted from the User Office Software.

User Community

The country of the home institute of investigators and co-investigators on each DEMAX proposal has been recorded over all four years of operation. There is a bias towards Sweden as ESS staff, often included in proposals, are all associated with Sweden. Indeed in 2025, this bias towards Sweden has increased in 2025, with the opening of calls for proposals specifically relating to early instrument commissioning for which ESS staff members had to be included.

Science Areas Impacted by DEMAX

Currently DEMAX prepares or helps prepare samples for users of neutron sources around the world. Since 2019, proposals have been received to address fundamental research questions and health, climate and environmental issues and issues in food, water and the bioeconomy. In 2025 one of the calls was specifically for proposals to generate samples for early science on ESS instruments. Requests for samples for NMX and LOKI were predominant, but proposals also included ESTIA, FREIA, HEIMDAL, MAGIC, MIRACLES, and the Test Beamline.

As in previous years, the main science techniques requiring deuterated samples were macromolecular crystal diffraction, reflectometry, small-angle neutron scattering, with two proposals for liquid and disordered material diffraction and one for engineering diffraction.

Figure 1. Number of Accepted Proposals by DEMAX Pillar

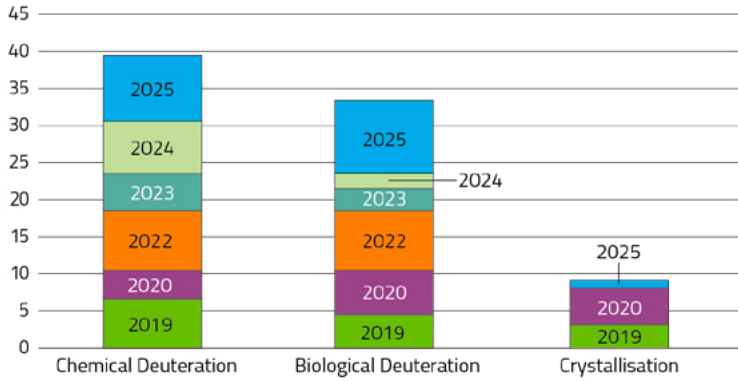
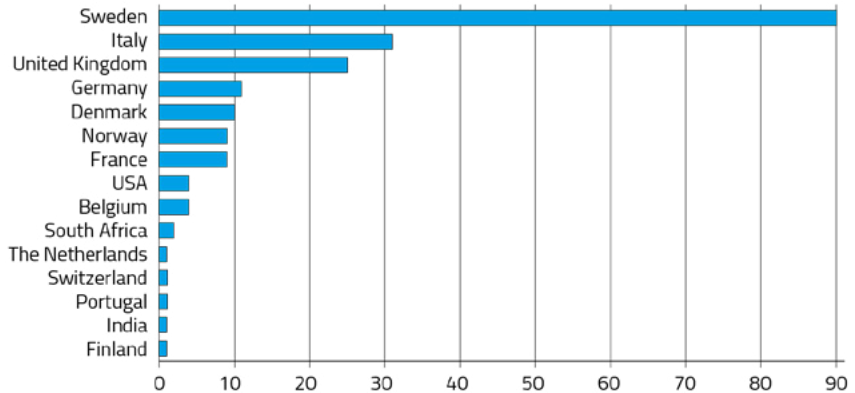


Figure 2. Number of Investigators per home institute



SCIENCE EVENTS

Seminars

The seminars delivered in 2025 can be split into three categories:

- **Science Café:** a seminar series connecting scientists at ESS
- **Ad hoc seminars:** seminars organised for ESS scientists and those in the local science community and given by visiting scientists at ESS
- **Interview seminars:** seminars given by candidates for jobs within the science directorate.

During 2025, Science Café seminars were delivered by:

- Anna Leung – Scientific Support Division
- Daria Noferini – Spectroscopy Division
- Mohamed Aouane – Spectroscopy Division
- Nico Paracini – Data Management and Scientific Computing Division
- Peyman Olad and Diego Herrera Ruiz – Accelerator Division
- Philipp Arnold – Accelerator Division
- Søren Schmidt – Data Management and Scientific Computing Division
- Thawatchart Chulapakorn – Diffraction and Imaging Division

Attendance at the seminars has ranged from 85 people to as few as 15 people, with an approximate average attendance of 25 people per seminar across the series.

In 2025, 17 ad hoc seminars were organised at ESS and DMSC, contributing to a dynamic and internationally connected scientific environment. These seminars typically attracted 10–50 participants per event and were attended by ESS staff as well as external scientists, both on-site and via online participation, reflecting broad interest and accessibility.

The seminar programme brought together speakers from leading universities, national laboratories, research institutes, and industry, covering a wide range of topics relevant to neutron science, materials research, energy, life sciences, and data-driven methodologies.

A particular highlight of the 2025 programme was a seminar delivered by Morten Meldal (University of Copenhagen), Nobel Laureate in Chemistry (2022), which significantly enhanced the scientific visibility and profile of the seminar series.

Seminars in 2025 were given by:

- Alessandra Luchini, University of Perugia
- Andreas Aakjær Andersen, Danish Technical Institute
- Cody Dennett & Jack Vargas, Commonwealth Fusion Systems
- Daniel Russo, Aalborg University
- Daniel S. Hussey, NIST
- Don Brown, LANL
- Erik van Loon, Lund University
- Felix Fernandez Alonso, Donostia International Physics Center and IKERBASQUE
- Jon Sporning, University of Copenhagen
- Luise Theil Kuhn, DTU Energy
- Martin Malmsten, University of Copenhagen
- Morten Meldal, University of Copenhagen
- Rebecca Anderson, ORNL
- Sophie Ayscough, Lund University
- Wojtek Potrzebowski, SciLifeLab Lund
- Yann Coppier, Lund University
- Zhou Shen, Max Planck Institute

Overall, the science seminars at ESS in 2025 supported knowledge exchange, interdisciplinary dialogue, and international collaboration, reinforcing ESS and DMSC as attractive hubs for scientific exchange and external engagement.

Events

In 2025, ESS played a central role in organising, hosting, and supporting a broad portfolio of high-profile scientific events, reinforcing its position as a key hub for the international neutron science community. These activities ranged from large international conferences to focused workshops, satellite meetings, and training events, addressing both scientific excellence and community building.

International Conference on Neutron Scattering (ICNS 2025)

In July 2025, ESS proudly hosted the International Conference on Neutron Scattering (ICNS 2025), one of the most significant global events in the neutron science calendar. The conference brought together more than 800 scientists from across the international neutron community.

The programme comprised three days of plenary and parallel talks, poster sessions, sponsor exhibitions, and networking events at Bella Center in Copenhagen, Denmark, followed by a dedicated fourth day at The Loop near ESS in Lund, Sweden. During this site visit, approximately 550 conference participants, supported by around 200 ESS volunteers, visited ESS to engage with the facility's progress.

The visit focused on the 15 neutron instruments under construction and commissioning, providing future users with first-hand insight into ESS capabilities and operational readiness. The event demonstrated ESS's strong commitment to delivering world-class instrumentation, comprehensive user support, and enabling high-impact science. ESS participation and scientific contributions included:

- 73 ESS registrations
- 63 posters (43 in Copenhagen; 20 at The Loop)
- Oral contributions and informal sessions at The Loop, including two exhibition stands, two dedicated rooms for informal discussions, and presentations in the auditorium.



ICNS took place at Bella Center in Copenhagen, and at The Loop and ESS in Lund, 6–10 July 2025.

Workshops, Mini-Symposia, and Satellite Meetings

In conjunction with ICNS 2025, ESS organised five mini-symposia and two satellite workshops, further enhancing the scientific depth and networking opportunities associated with the conference.

A number of targeted scientific meetings were organised in connection with ICNS 2025, enabling focused discussion on emerging topics and technical challenges:

- Commissioning of Neutron Scattering Instrumentation (ESS/ORNL) – closed mini-symposium enabling exchange of lessons learned between ESS and SNS TS-2
- Deuteration Matters – hosted by DeuNet, highlighting the strategic role of deuteration facilities
- Magnetic SAS Data Analysis – State of the Art and Future Improvements – community discussions and teaching activities around data analysis tools
- Modelling Coherent Excitations – specialist satellite workshop leveraging the presence of international experts
- Advanced Computer Simulation Methods for Neutron Scattering Instruments – satellite workshop addressing simulation tools for instrument optimisation and experiment support.

An additional closed satellite workshop was hosted later in the week, further strengthening expert-level exchange.

Data, Software, and Community-Driven Events

SciCatCon 2025

In July 2025, the ESS Data Management and Scientific Computing Centre (DMSC) hosted SciCatCon 2025, the fourth in-person meeting dedicated to SciCat, the scientific metadata catalogue. As a leading partner in the SciCat project, ESS used this event to consolidate its leadership role within the community. The workshop provided a forum for users and developers to exchange feedback, discuss technical architecture and deployment solutions, explore new features and user-developed applications, and address data curation challenges across facilities.

DMSC Summer School

The DMSC Summer School, held in August 2025 in Copenhagen and Lund, focused on training students and early-career researchers to use the ESS DMSC software for neutron-scattering data workflows. Participants worked with simulated instrument data, performing data reduction, analysis, and open data storage. The school generated strong engagement, with many participants planning to adopt the tools within their

home institutions. Twenty researchers and students participated, PhD student, Postdoc, PhD fellows, Master students, Researchers and Associate professors, from universities and facilities across Europe.

Scientific Python Developer Summit

In November 2025, ESS hosted the Scientific Python Developer Summit, bringing together developers from major open-source scientific software projects. The event supported collaboration on shared infrastructure, project sustainability, and long-term strategy for the scientific Python ecosystem.

Through its engagement in large international conferences, specialised workshops, satellite meetings, and training activities, ESS significantly contributed to scientific exchange, skills development, and international collaboration in 2025. These events strengthened ESS's visibility, supported future user communities, and aligned closely with ESS's strategic objectives in science, data, and infrastructure development.



The final day of ICNS was spent at The Loop and at ESS in Lund.

GRANTS ACTIVITIES

As of 31 December 2025, ESS has 24 ongoing projects (Table 1). This represents an increase of six projects compared with the year-end total for 2024, when 16 projects were active.

Additionally, 2025 saw a record number of 69 submitted proposals (Table 2), reflecting a strong and growing interest in grant-related activities.

This growth reflects the continued expansion of ESS related grant activities and collaborations. The increase in the grants portfolio also indicates a broadening scientific, technical and partnership engagement as we prepare for First Science.

Cooperation with ISIS – Grants Highlight

In 2025, Vetenskapsrådet (The Swedish Research Council) launched a call titled “Cooperation with ISIS; instrumentation and method for ESS.”

The aim of the call is to strengthen collaboration between UK and Swedish researchers while preparing research groups for the early use of the first instruments at ESS. ESS instrument scientists, together with their respective partners at ISIS, submitted a total of 12 applications under this call.

The collaborative projects are expected to advance or apply neutron science, enhance capabilities at both ISIS and ESS, and engage new user groups and researchers in neutron-based methods. In particular, the projects focus on developing the capabilities of the first suite of seven instruments at ESS. This includes work on novel instrumentation, sample environments, methodologies, analysis methods, and software. The overall objective is to support and contribute to the early science programme at ESS during the project period.

This initiative is important for the development of new technologies and instruments at ESS and will provide the Swedish research community with early experience and the necessary expertise to take full advantage of the unique opportunities ESS will offer. The partnership with ISIS enables researchers in Sweden and the UK to fully benefit from both facilities, particularly in strengthening scientific and technical expertise in neutron scattering for advanced materials research.

Table 1. Snapshot of Ongoing Projects as of December 2025

Funder and ESS Role	ESS Budget (EUR)	# of Projects
Chalmers University	217 945,00	1
Beneficiary	217 945,00	1
European Commission (EC)	4 358 444,00	13
Beneficiary	2 397 719,00	12
Coordinator	1 960 725,00	1
Vetenskapsrådet (VR)	379 651,00	3
Beneficiary	379 651,00	3
OSCARs Programme	249 950,00	1
Beneficiary	249 950,00	1
HALRIC Programme	-	5
Beneficiary	-	5
Innovation Fund Denmark	113 103,00	1
Beneficiary	113 103,00	1
Grand Total	5 319 093,00	24

Table 2. Snapshot of ESS Proposal Submission from 2025

Funder	ESS Budget (EUR)	# of Projects
Successful	325 877,00	10
European Commission (EC)	36 539,00	2
HALRIC Programme	31 649,00	4
Vetenskapsrådet (VR)	257 689,00	3
Univ.of the Basque Government	-	1
Unsuccessful	1 120 816,00	18
Vetenskapsrådet (VR)	831 600,00	11
Innovation Fund Denmark	289 216,00	1
Formas	-	5
Swedish Foundation for Strategic Research (SSF)	-	1
In Evaluation	6 165 146,00	41
Danish Agency for Science, Technology and Innovation (DASTI)	1 727 264,00	2
European Commission (EC)	2 045 687,00	10
Nordforsk	-	3
Novo Nordisk Foundation	244 572,00	1
Vetenskapsrådet (VR)	2 147 623,00	25
Grand Total	7 611 839,00	69

SCIENTIFIC PUBLICATIONS

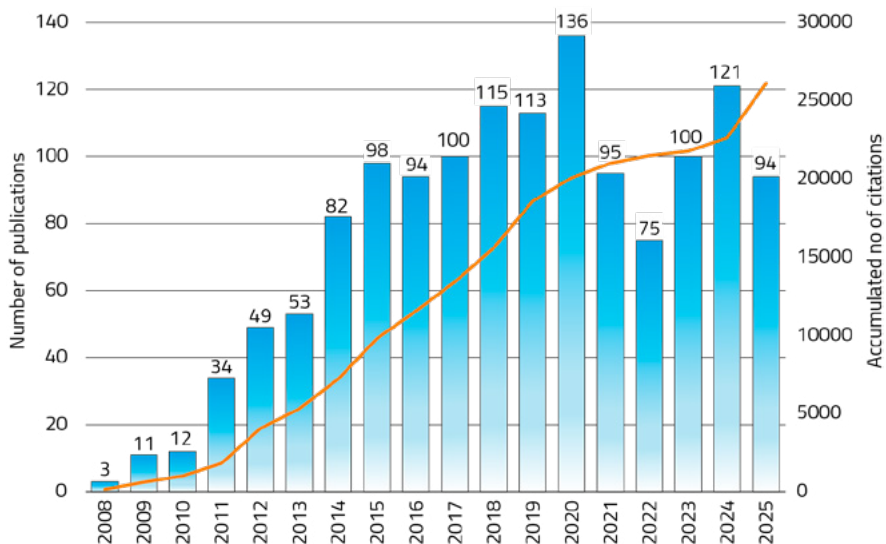
Total Publications

The method used to trace publications involving ESS is based on the affiliation metric offered by Scopus. Scopus builds institution profiles from the affiliation text in the articles it indexes. Scopus algorithms can identify name variations and link them into one profile. Affiliation IDs are assigned to the “parent” institution, as well as any “child” institutions in the institution’s hierarchy. Due to the great variation in the way affiliations are represented by authors and publishers, this automated process can never be exact. Some variants may be missed, and others may be inappropriately included. When identified, erroneous entries are removed manually. Additionally, to avoid missing publications, researchers are encouraged to inform the library staff when they have publications not expected to be found through the common channels. Such publications might be related to conferences and other non-journal activities.

The total number of publications published by ESS affiliates during 2025 is 94. This number includes data from Scopus as well as data from researchers at ESS.

The ESS encourages its scientists to publish in Open Access journals and 2025, 74% of 2025 publications were Open Access. The all-time figure is 52%.

Figure 3. Total publications per year



Total Citations

The cohort of 94 papers published in 2025 received 96 citations during the same year. The complete set of ESS publications received 3224 citations from other scientific publications during 2025. Over all-time, publications affiliated with researchers at ESS have been cited a total of 26115 times and are cited more than 8 times a day on average.

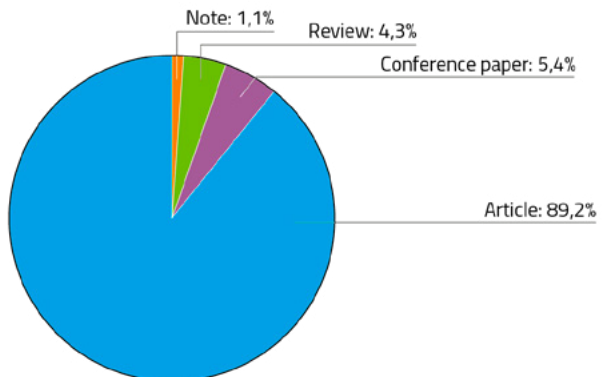
H-index

Having identified all the publications for a given year the H-index has been taken from the data included in Scopus. The H-index means that there are h papers that have been cited at least h times and therefore gives an indication of the scientific impact of the publications. Using the complete set of ESS publications, ESS has an all-time H-index of 72. In other words, we have 72 publications that are cited at least 72 times. The equivalent metric reported for 2024 was 68.

Type of Publication

During 2025, we see a surprising decrease of the number of Conference Papers. During COVID we saw a natural decline in the number of conference papers. Post-COVID the numbers have increased annually from 8,3% to 14,9% in 2024. Still a far reach from the 38% we had between 2017 and 2019. It will be interesting to track the evolution of these numbers and see if it is a trend or an anomaly.

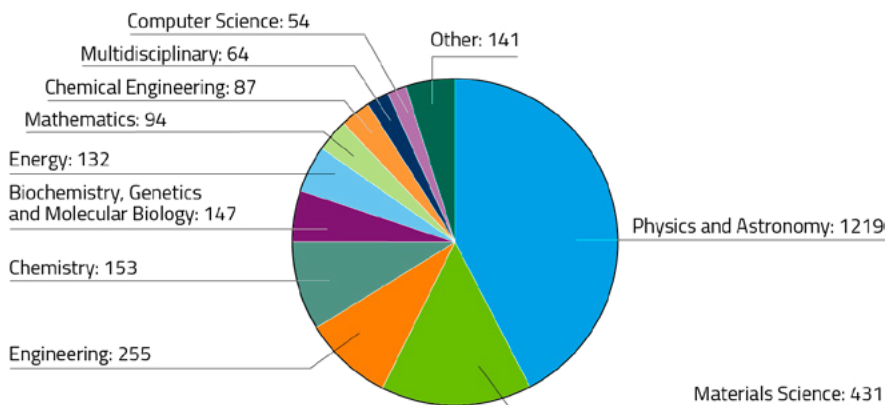
Figure 4. Type of publication



Distribution of Research Categories 2025

The distribution of research categories in papers published during 2025 gives an idea of the broadness of disciplines represented at ESS.

Figure 5. Distribution of Research Categories



Authors by country affiliation

Data is shown for authors by country, for the top 15 countries. All documents will have Sweden as the author country since affiliation with ESS is counted as Swedish. For this reason, Sweden is removed for ease of reading.

Publications in Top Citation Percentile

For this metric, the citation count of the publication is compared to the whole cohort of publications in the same field and the same year. Those publications that are cited as many times as the top 10% are considered to be most impactful.

Since citations accrue over time, this metric will be carried out for a 10-year period, ending one year before 2025. During this span, ESS has had 119 publications in the top 10% of cited journals, which is an average of 9.6% of all our articles. The orange in each column indicates publications in 1% most cited.

Publications in Top Journal Percentile

Publications in Top Journal Percentiles in SciVal indicates the extent to which an entity's publications are present in the most-cited journals in the data universe. The blue indicates top 10% of the most cited journals, while orange indicates top 1%. ESS has on average 22.9% of its articles published in top 10% cited journals for the given period, which is well above the expected.

Figure 6. Authors per country affiliation

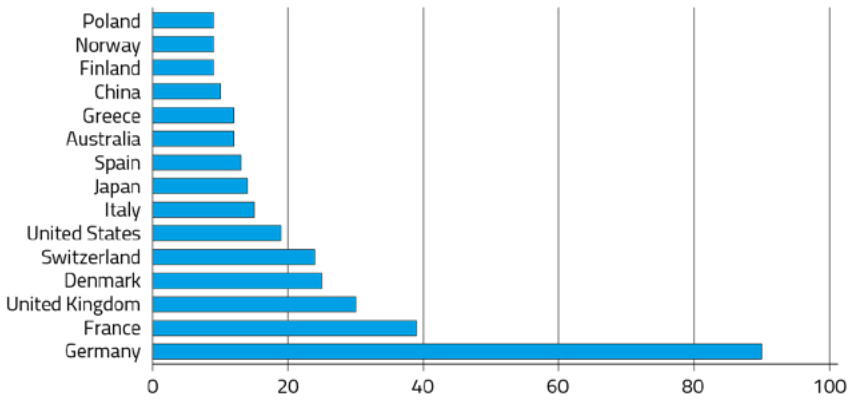


Figure 7. Publications in Top Citation Percentile

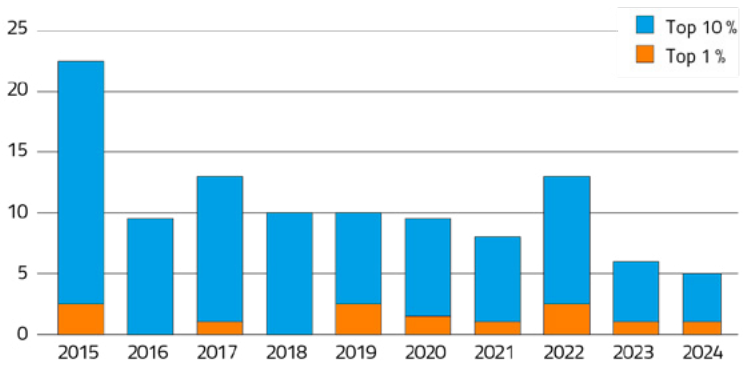
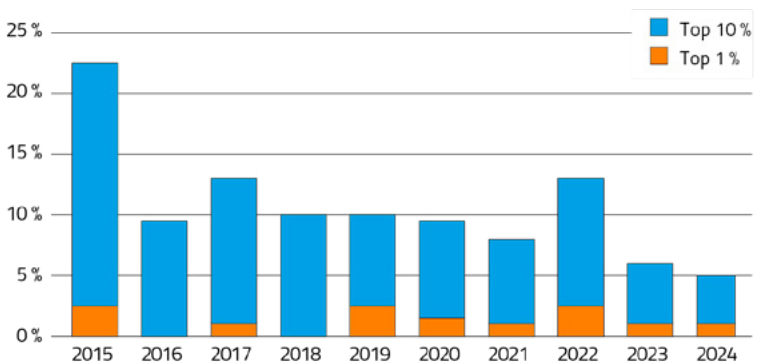


Figure 8. Publications in Top Journal Percentile



Most Cited Papers

To find the most cited papers, a cross-reference between Scopus and Google Scholar was carried out. The number usually differs significantly due to Google Scholar being more inclusive in the resources it collects data from. Scopus, a curated data source, has selectivity about what types of resources are included. One could argue that data from Google Scholar is less reliable due to its inclusive nature. One could also argue that it is more reliable due to its inclusivity. The same could be said about Scopus and its exclusive nature. Each set of numbers needs to be analysed in its own context – perhaps taken together, they create a more truthful picture.

From the papers published in 2025 is a paper published on the second to last day of 2024. Since it had no chance of citations in 2024 it is included here. It received 30 citations in Google Scholar and 12 in Scopus:

- McCluskey, Andrew R., Samuel W. Coles, and Benjamin J. Morgan. "Accurate estimation of diffusion coefficients and their uncertainties from computer simulation." *Journal of Chemical Theory and Computation* 21.1 (2024): 79-87.
- If we want to disregard the mentioned paper due to its 2024 relation, the most cited paper published in 2025, with 15 citations in Google Scholar and 8 in Scopus, is:
- Arora, M. M., et al. "Search for Light Dark Matter with NEWS-G at the Laboratoire Souterrain de Modane Using a Methane Target." *Physical Review Letters* 134.14 (2025).
- From all papers published by ESS affiliates, the most highly cited paper, with 1115 citations in Google Scholar and 848 in Scopus, is:
- Abada, A. E. A., Arias, S. et al. "FCC-ee: the lepton collider: future circular collider conceptual design report volume 2." *The European Physical Journal Special Topics* 228 (2019): 261-623.

January | 2025 HIGHLIGHTS

Concurrent operando neutron imaging and diffraction analysis revealing spatial lithiation phase evolution in an ultra-thick graphite electrode.

This study presents a novel operando methodology combining neutron imaging and diffraction to investigate lithiation dynamics in ultra-thick graphite electrodes for lithium-ion batteries. Addressing challenges associated with thick electrodes—such as transport limitations and heterogeneous lithiation—the authors use a time-of-flight diffractometer at J-PARC equipped with a retrofitted imaging detector. This setup enables simultaneous, spatially resolved measurements of lithium content and intercalation phases during the battery's first charge-discharge cycle. Key findings include the co-existence of multiple lithiation phases during cycling, delayed lithiation and delithiation in the electrode centre, and concentrated solid electrolyte interphase (SEI) formation near the separator.

The integration of diffraction and imaging reveals both crystallographic lithium phases (e.g., LiC₁₂, LiC₆) and non-intercalated lithium (e.g., dead Li, SEI), offering comprehensive insight into lithium distribution and kinetics. The study identifies a significant irreversible capacity loss linked to trapped lithium in low-concentration Li–C phases such as LiC₃₆ and LiC₇₂. The technique not only enables quantification of lithium phase evolution across electrode thickness and time but also demonstrates potential for application in the study of fast-charging behaviour. This multimodal approach advances the understanding of electrochemical limitations in thick graphite electrodes, which are central to next-generation high-energy-density battery designs.

Citation: Strobl, M., Baur, M. E., Samothrakitis, S., Malamud, F., Zhang, X., Tung, P. K. M., Schmidt, S., Woracek, R., Lee, J., Kiyonagi, R., Kuhn, L. T., Segev, I. G. & Ein-Eli, Y. Concurrent operando neutron imaging and diffraction analysis revealing spatial lithiation phase evolution in an ultra-thick graphite electrode. *Adv. Energy Mater.* 15, 2405238 (2025).
<https://doi.org/10.1002/aenm.202405238>

ESS Contact: Robin Woracek

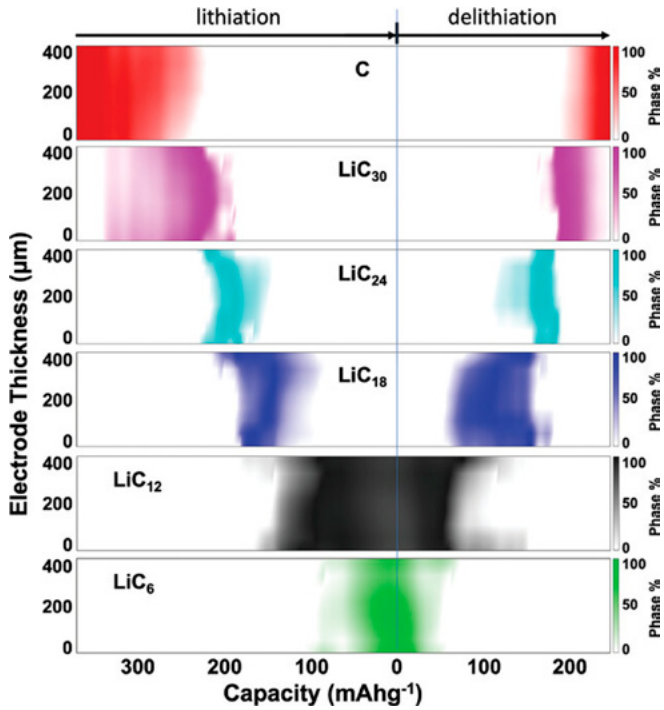


Figure 9. Phase evolution against electrode thickness throughout cycling. This figure visually encapsulates the core finding: the spatially and temporally resolved progression of individual lithiation phases (LiC₃₀ to LiC₆) across the ultra-thick electrode during battery cycling.



February | 2025 HIGHLIGHTS

Raman microspectroscopy to trace the incorporation of deuterium from labelled (micro)plastics into microbial cells.

This study introduces a powerful new application of stable isotope Raman microspectroscopy (SIRM) to trace the assimilation of deuterium from labelled microplastics into microbial biomass at the single-cell level. The researchers synthesised D-lactic acid-d₄, and from this produced perdeuterated polylactic acid (dPLA), as a model bioplastic to investigate its microbial degradation under environmentally relevant conditions. The uptake of deuterium into lipids, proteins, DNA, and carotenoids was monitored via Raman-active C–D vibrational modes, offering insights into metabolic pathways during plastic biodegradation. SIRM enabled phenotypic classification of *Sphingomonas koreensis* into labelled and unlabelled populations and revealed distinct patterns of biomolecular deuteration depending on the source (dPLA vs glucose-d₁₂ or D₂O), supporting the hypothesis that microbial metabolism depends on polymer breakdown products.

Importantly, this method was extended to a soil bacterial consortium, confirming the transferability of the approach to complex environmental systems. Strong deuterium uptake was observed after two weeks, with three distinct cell populations indicating active degraders, inactive species, and potentially cross-feeding microbes. Resonance Raman spectroscopy targeting carotenoids in *S. koreensis* further enhanced the method's sensitivity and throughput, allowing detection of D-label incorporation with short acquisition times. This multimodal vibrational approach offers a cost-effective and scalable alternative to isotope mass spectrometry for tracking plastic biodegradation and has the potential to identify degrading species, quantify assimilation pathways, and assess the environmental fate of emerging biodegradable polymers.

Citation: Müller, K., Elsner, M., Leung, A. E., Wacklin-Knecht, H., Allgaier, J., Heiling, M. & Ivleva, N. P. Raman microspectroscopy to trace the incorporation of deuterium from labelled (micro)plastics into microbial cells. *Anal. Chem.* 97, 4440–4451 (2025). <https://doi.org/10.1021/acs.analchem.4c05827>

ESS Contact: Hanna Wacklin-Knecht

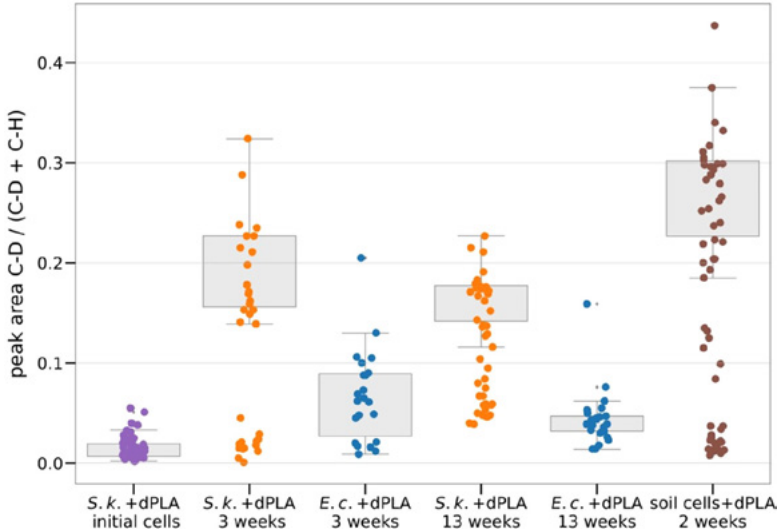


Figure 10. Temporal changes of single-cell deuterations during incubation with dPLA. This figure summarises a key result – phenotypic heterogeneity in deuterium uptake over time – providing a clear visual of SIRM’s ability to resolve cell-level dynamics during microplastic biodegradation. This figure highlights both the method’s power and the complexity of microbial responses.



March | 2025 HIGHLIGHTS

Structural and magnetic characterization of Fe–Ga thin films sputter-deposited on Si wafers and optical fibres.

This study presents a comparative structural and magnetic characterisation of Fe–Ga (galfenol) thin films sputter-deposited onto flat Si(100) wafers and cylindrical optical fibre Bragg gratings (FBGs), aimed at enabling magnetostrictive sensing applications. Using two deposition geometries—‘base’ and ‘rôtisserie’—the authors explore how substrate shape and orientation relative to the target affect film morphology and properties. Structural analyses using scanning electron microscopy (SEM), energy dispersive X-ray spectroscopy (EDS), and X-ray diffraction (XRD) revealed that the films exhibit a columnar morphology and are predominantly in the disordered body-centred cubic (A2) phase, with a preferred (111) growth orientation. The column orientation and film texture varied with deposition configuration, with more uniform coatings and vertical columns observed for the optical fibres in the *rôtisserie* setup.

Magnetic characterisation via hysteresis loops and first-order reversal curves (FORCs) demonstrated that the films support a mix of magnetic single and multi-domains, with strong anisotropy linked to the columnar structure. Across both substrate types, magnetic easy axes aligned parallel to the film surface, while hard axes lay perpendicular. Notably, the wafer-R sample, which had inclined columns, exhibited unique magnetic signatures with implications for sensor design. Overall, the study confirms that Fe–Ga thin films can be reproducibly deposited onto cylindrical fibre substrates with properties comparable to those on flat wafers, supporting the development of high-sensitivity magnetostrictive FBG-based sensors.

Citation: Durniak, C., Foster, S. & Bulla, D. Structural and magnetic characterization of Fe–Ga thin films sputter-deposited on Si wafers and optical fibres. *Sens. Actuators A Phys.* 383, 116222 (2025). <https://doi.org/10.1016/j.sna.2025.116222>

ESS Contact: Celine Durniak

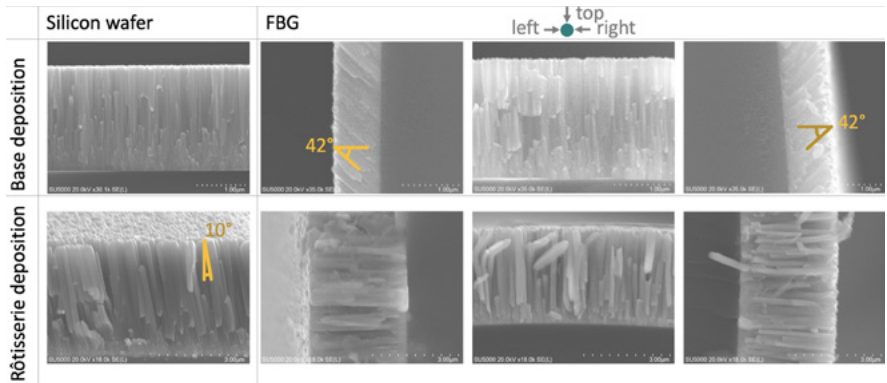


Figure 11. SEM images of the thin film cross sections. This figure visually highlights the core structural insight: the columnar morphology and its orientation depending on substrate type and deposition geometry. The figure powerfully illustrates the microstructural basis for the magnetic properties discussed throughout the paper.



April | 2025 HIGHLIGHTS

Membrane Charge Drives the Aggregation of TDP-43 Pathological Fragments.

On of TDP-43 pathological fragments, with a focus on their relevance to neurodegenerative diseases. Extracellular vesicles (EVs), including exosomes and microvesicles, are discussed as significant carriers of lipids, proteins, and genetic material, facilitating intercellular communication and contributing to both physiological and pathological processes in the central nervous system. The study specifically examines how TDP-43 fragments, including M85, interact with these membrane structures and the implications for disease progression.

Experimental data in the article reveal that aggregation of TDP-43 fragments is influenced by membrane lipid composition, demonstrating an inverse correlation between Thioflavin T (ThT) fluorescence (a marker for protein aggregation) and the levels of soluble protein remaining in solution. These findings indicate that membrane charge can promote pathological aggregation, potentially like mechanisms described for other neurodegeneration-related proteins like α synuclein. Notably, the study highlights the occurrence of aggregates too small to be separated under standard centrifugation, suggesting unique aggregation behaviours depending on lipid environment. These insights advance our understanding of the molecular underpinnings of TDP-43 pathology and the broader role of EVs in neurodegenerative disease contexts.

Citation: Corucci, G. Vadukul, D.M., Paracini, N., Laux, V., Batchu, K.C., Aprile, F.A., and Pastore A., Membrane charge drives the aggregation of TDP-43 pathological fragments. *J. Am. Chem. Soc.*, 147, 13577-13591 (2025) <https://pubs.acs.org/doi/10.1021/jacs.5c00594>

ESS Contact: Nicolò Paracini

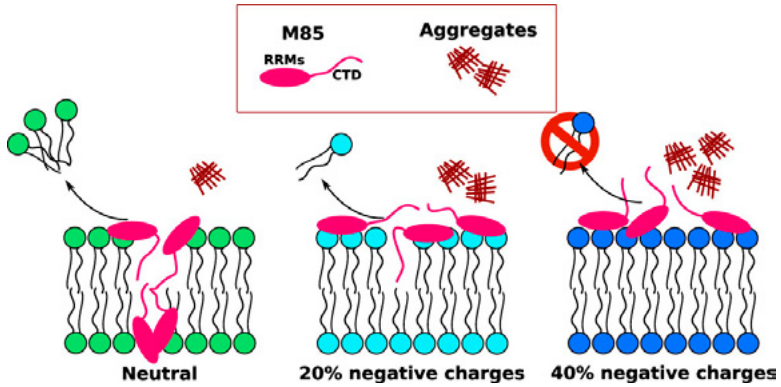


Figure 12. On neutral membranes, M85 inserts into the bilayer and causes membrane disruption with limited aggregation. Increasing membrane negative charge shifts M85 toward surface binding, promotes protein aggregation, and reduces bilayer damage. These results suggest that membrane charge may modulate TDP-43 aggregation and membrane-associated pathology in neurodegenerative disease.



May | 2025 HIGHLIGHTS

Exploring grain-resolved strain tensors and non-uniform lattice deformations with Laue 3DNDT.

This study presents a novel application of Laue three-dimensional neutron diffraction tomography (Laue 3DNDT) to measure grain-resolved strain tensors and orientation changes in an oligocrystalline Co-Ni-Ga shape-memory alloy subjected to in situ compressive loading. Leveraging the high penetration depth of neutrons, Laue 3DNDT enables non-destructive, high-throughput characterisation of elastic strain evolution across individual grains within the bulk material. Strain tensors were determined for seven of the eleven indexed grains with a resolution of $\sim 10^{-3}$ over an applied strain range of 0–2%. The experimental results revealed heterogeneous strain distributions and anisotropic responses at the grain scale, influenced by grain orientation, size, and intergranular interactions. This was particularly evident from differences in the principal strain components and reorientation behaviour across grains, even in the nominally elastic regime.

To validate and interpret these findings, results were compared with both single-crystal elasticity models and elasto-viscoplastic Fast Fourier Transform (EVPFFT) simulations. While the single-crystal models captured orientation-dependent elastic behaviour, they failed to account for intergranular constraints. In contrast, EVPFFT simulations, incorporating detailed microstructural morphology, showed good agreement with the experimental grain-averaged strain data, though some deviations remained, likely due to microstructural features such as γ -phase precipitates and the limitations of voxel resolution. The study demonstrates the unique capability of Laue 3DNDT to resolve strain and orientation distributions in situ, with implications for developing and validating predictive models of mesoscale deformation in functional materials.

Citation: Larsen, C. B., Samothrakitis, S., Woracek, R., Polatidis, E., Čapek, J., Upadhyay, M. V., Tovar, M., Schmidt, S. & Strobl, M. Exploring grain-resolved strain tensors and non-uniform lattice deformations with Laue 3DNDT. *Acta Mater.* 289, 120869 (2025).
<https://doi.org/10.1016/j.actamat.2025.120869>

ESS Contact: Robin Woracek

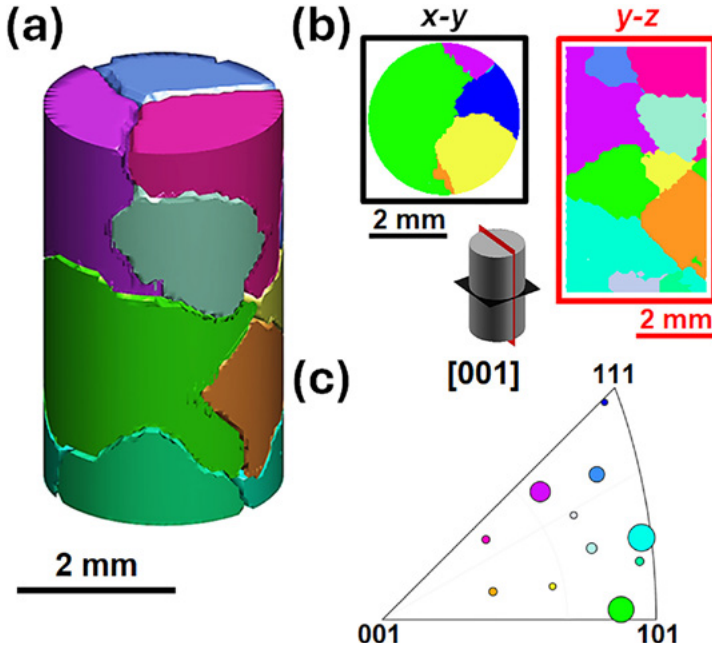


Figure 13. Morphological map of the sample volume obtained from the indexed centre-of-mass positions in (a) isoprojection and (b) along the x-y and y-z planes, in accordance to the schematic in the figure. The relative volume of each grain is fixed to match their relative average intensity among the indexed grains. (c) Inverse pole figure (IPF) map containing the orientations of the 11 indexed grains of the Co-Ni-Ga sample, where [001] corresponds to the loading direction. The sizes of the circles reflect the relative grain-sizes, again determined from their relative average spot intensity. The grains are colour-coded according to their orientations.



June | 2025 HIGHLIGHTS

Dynasor 2: From simulation to experiment through correlation functions

The authors discuss the application of molecular dynamics (MD) simulations to gain detailed insights at the atomic scale, which is crucial in physics, chemistry, and materials science. MD simulations generate trajectories of atomic positions and velocities, enabling researchers to compute both structural and dynamical properties of materials. A central theme of the paper is the use of correlation functions derived from these MD trajectories - such as static and dynamic structure factors, current correlations, and spectral energy density (SED) - which provide direct links to experimentally observable properties and deepen understanding of material behaviour at the atomic level.

The text introduces version 2.X of the dynasor package, which is a major upgrade over the 1.X release. The new version offers a fast, unified, Python-based interface for computing a wider range of autocorrelation functions (ACFs) from molecular dynamics (MD) trajectories. dynasor 2.X now supports probe-specific weighting factors, including X-ray, neutron, and electron form factors and scattering lengths, allowing for accurate computation of scattering patterns across multiple probe types. It also integrates advanced analysis tools like mode projection, providing deeper insight into atomic dynamics, and is supported by comprehensive online documentation.

Citation: Berger, E., Fransson, E., Eriksson, F., Lindgren, E., Wahnström, G., Holm Rod, T., Erhart, P. Dynasor 2: From simulation to experiment through correlation functions. *Comput. Phys. Commun.* 316, 109759 (2025). <https://doi.org/10.1016/j.cpc.2025.109759>

ESS Contact: Thomas Holm Rod

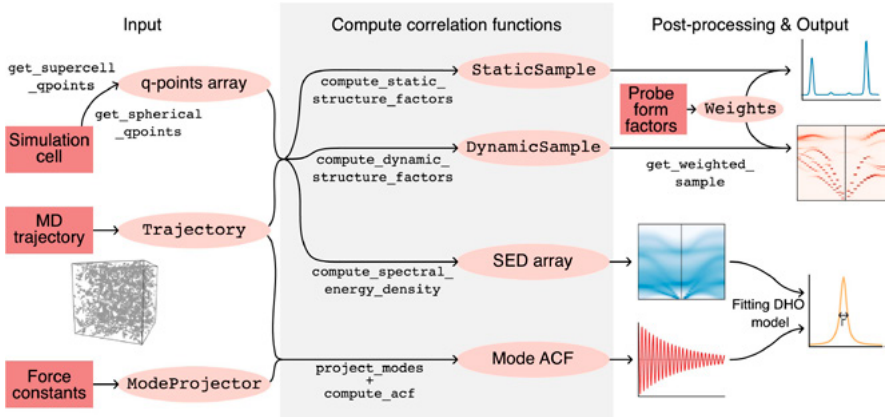


Figure 14. The dynasor workflow typically consists of three parts: input, computation of the correlation functions, and handling of the output, which can include post-processing steps. The key component of the user input is a MD trajectory, which is parsed via dynasor trajectory readers. In addition, a simulation cell or force constants are required, depending on which correlation functions are to be computed.



July | 2025 HIGHLIGHTS

Off-target binding of the histone deacetylase inhibitor vorinostat to carbonic anhydrase II and IX

Histone deacetylase inhibitors (HDACi) such as vorinostat (SAHA) are widely used in cancer therapy but often exhibit off-target effects due to their interaction with other zinc-dependent enzymes. This study reports high-resolution crystal structures of SAHA bound to human carbonic anhydrase II (CA II) and a CA IX active-site mimic, revealing previously uncharacterised off-target binding.

Structural analyses at room temperature and cryogenic conditions show that SAHA adopts two conformations within the CA active sites, coordinating the zinc ion through its hydroxamate group in tetrahedral or pentahedral geometries while displacing catalytic water molecules. Differences in binding between CA II and the CA IX mimic are linked to local residue variation, particularly the Phe131→Val substitution, which alters hydrophobic interactions and increases ligand flexibility. Docking predictions were consistent with crystallographic observations, and thermal-shift assays indicated minimal stabilisation of CAs by SAHA compared with classical sulfonamide inhibitors. Binding-energy calculations suggest affinities comparable to those for HDAC targets, supporting a potential contribution of carbonic anhydrase binding to clinical side effects.

The results highlight the structural basis of SAHA off-target interactions and suggest that hydroxamate scaffolds could serve as alternatives for designing carbonic anhydrase inhibitors, although isoform selectivity remains challenging. In the reported X-ray structures there is some ambiguity in the ligand pose that was not possible to resolve using X-rays alone. Our next steps are to optimize the crystals for neutron studies and to use deuterated vorinostat (SAHA) prepared by the ESS Deuteration Group. Neutrons will allow us to use density for the H atoms to guide unambiguous placement and correct modelling of the ligand.

Citation: Gulkis, M. C., Hodgkinson, J. T., Sele, C. P., Knecht, W., McKenna, R. & Fisher, S. Z. Off-target binding of the histone deacetylase inhibitor vorinostat to carbonic anhydrase II and IX. *Acta Crystallographica Section F* 81, 388–397 (2025). <https://doi.org/10.1107/S2053230X25007447>

ESS Contact: Zoë Fisher

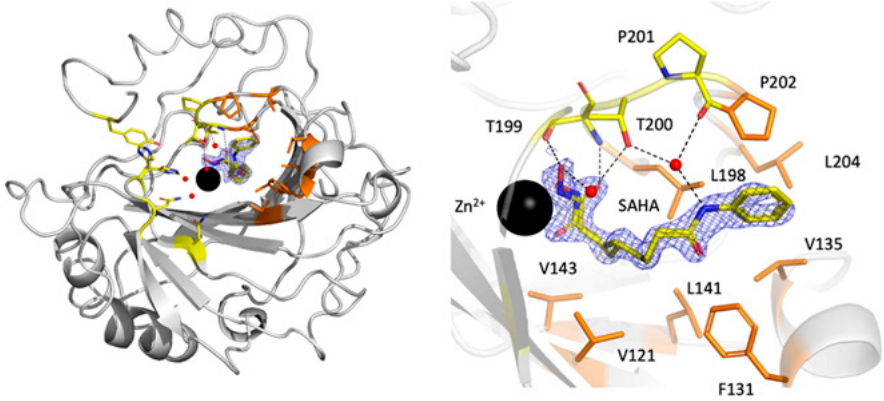


Figure 15. Binding interactions between CA II and SAHA. The CA II structure is shown in grey; the active-site Zn²⁺ and water molecules are shown as black and red spheres. Active-site residues and SAHA are shown in yellow ball-and-stick representation. Hydrophobic residues around the SAHA alkyl chain and benzene ring are shown in orange.



August | 2025 HIGHLIGHTS

Crystal-Symmetry-Driven Build Orientation and its Impact on the $\{110\}<100>$ Goss Texture Formation and Mechanical Properties of Laser Powder Bed Fused AISI 316L.

This study investigates how crystal-symmetry-driven build orientation influences crystallographic texture formation, microstructure, and mechanical properties of laser powder bed fused (PBF-LB/M) AISI 316L stainless steel. Using bi-directional scanning, the authors exploit the cubic symmetry of the fcc lattice to fabricate parts with an identical predominant $\{110\}<100>$ Goss texture but distinct thermal histories and melt pool morphologies along three build orientations: horizontal (H110), tilted (T110), and vertical (V110).

Bulk texture and phase composition were characterised using neutron diffraction, complemented by optical and electron microscopy, EBSD, and tensile testing. All samples were fully dense (>99.9%) and single-phase austenitic. Despite sharing the same nominal Goss texture, significant differences were observed in texture strength, solidification structure, and mechanical response. The T110 orientation exhibits the strongest texture, a crystallographic lamellar microstructure with major $\{110\}$ and minor $\{111\}$ grains, and the finest cellular solidification structure.

Mechanically, T110 shows superior yield strength and ultimate tensile strength compared to H110 and V110 while maintaining high ductility (~45% elongation). Detailed microstrain and dislocation density analyses indicate that differences in strength are not primarily governed by dislocation density or grain boundary character. Instead, the refinement of the solidification structure, linked to orientation-dependent thermal gradients and interface velocities, is identified as the dominant strengthening mechanism.

Citation: Rainer, D., Marattukalam, J. J., Karlsson, D., Beran, P., Hervoches, C., Andersson, G., Pant, P. & Sahlberg, M. Crystal-symmetry-driven build orientation and its impact on the $\{110\}<100>$ Goss texture formation and mechanical properties of laser powder bed fused AISI 316L. *Adv. Eng. Mater.* 27, 2500423 (2025). <https://doi.org/10.1002/adem.202500423>

ESS Contact: Zoë Fisher

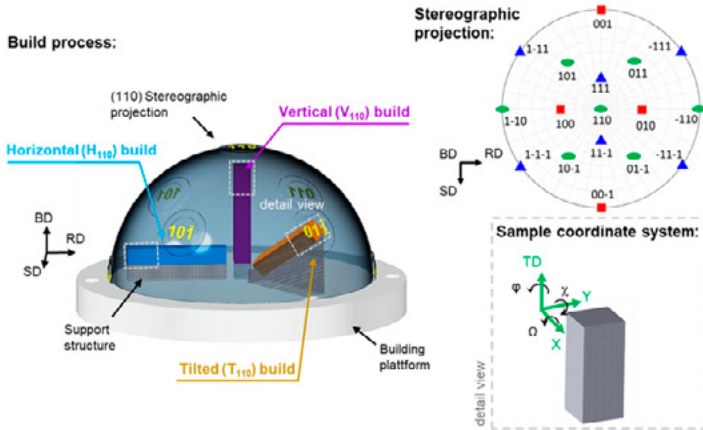


Figure 16. A schematic illustration of the build process including the $\{110\}$ stereographic projection. In black, the print coordinate system is shown with the build direction (BD), scan direction (SD), and re-coating direction (RD). The green sample coordinate system reveals the tensile direction (TD) parallel to the longitudinal axis, as well as X and Y.



September | 2025 HIGHLIGHTS

Magnetic monopole relaxation effects in spin ice $\text{Dy}_2\text{Ti}_2\text{O}_7$

This paper investigates magnetic monopole relaxation dynamics in the classical spin-ice compound $\text{Dy}_2\text{Ti}_2\text{O}_7$ using AC calorimetry as a probe of dynamic heat capacity. Spin-ice systems host emergent magnetic monopole excitations whose slow dynamics can strongly influence thermodynamic measurements, particularly at low temperatures. The authors measure the heat capacity over a temperature range of 0.5–5 K and modulation frequencies from 0.01 to 500 Hz, enabling access to relaxation timescales that are difficult to probe with conventional techniques.

A pronounced frequency dependence of the heat capacity is observed below approximately 2 K. At low frequencies, the heat capacity approaches the static value and displays the characteristic spin-ice peak near 1 K. As the frequency increases, this peak is progressively suppressed and shifts to higher temperature, with the high-frequency limit dominated by phononic contributions. From the frequency dependence, a characteristic relaxation time is extracted, showing a strong divergence on cooling and reaching values of around 6 s at 0.65 K.

Thermal transport modelling demonstrates that the observed behaviour cannot be attributed to finite thermal conductivity or sample inhomogeneity. Instead, dynamic Monte Carlo simulations of the dipolar spin-ice model reproduce the experimental frequency response, confirming that the effect originates from slow magnetic monopole dynamics. The simulations yield an effective timescale of approximately 20 ms per Monte Carlo step at 4 K, differing from previous estimates based on other experimental techniques.

Citation: Edberg, R., Khansili, A., Fjellvåg, I. M., Ørdu Sandberg, L., Deen, P. P., Lefmann, K., Henelius, P. & Rydh, A. Magnetic monopole relaxation effects in spin ice $\text{Dy}_2\text{Ti}_2\text{O}_7$. *Phys. Rev. B* 112, 094435 (2025). <https://doi.org/10.1103/PhysRevB.112.094435>

ESS Contact: Zoë Fisher

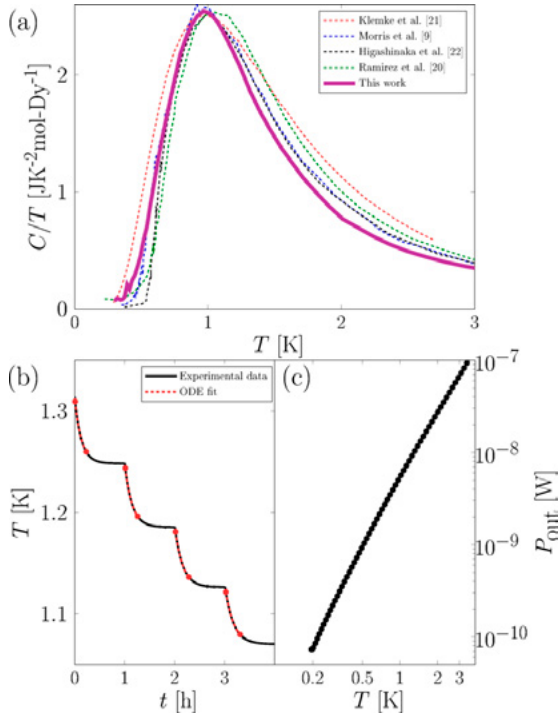


Figure 17. Heat capacity and thermal-relaxation properties of a DTO powder sample cold pressed with silver powder. (a) Our heat capacity values compared with four data sets from the literature. (b) Thermal relaxation which has been fitted to determine $C(T)$ shown in red. (c) Experimentally measured P_{out} as function of temperature.



October | 2025 HIGHLIGHTS

In hospite and *ex hospite* architecture of photosynthetic thylakoid membranes in *Symbiodinium* spp. using small-angle neutron scattering.

This study demonstrates that small-angle neutron scattering (SANS) can be used to resolve the native architecture of photosynthetic thylakoid membranes in live symbiotic dinoflagellate algae (*Symbiodinium* spp.), both extracted from their hosts (*ex hospite*) and within living host tissue (*in hospite*). The work establishes a non-destructive structural probe for investigating thylakoid organisation in coral symbioses, with direct relevance to understanding mechanisms underlying coral bleaching.

SANS measurements were performed on live *Symbiodinium* associated with the coral analogue *Aiptasia* and the reef-building coral *Acropora*. To interpret the scattering data, the authors developed a biologically realistic triple-vesicle model representing stacked thylakoid triplets, guided by transmission electron microscopy and constrained by known biochemical compositions. This model successfully reproduces key scattering features across all experimental conditions and yields quantitative structural parameters, including bilayer thicknesses, lumen widths and inter-thylakoid (IT) gap spacings.

A targeted sensitivity and covariance analysis shows that the approach can resolve IT-gap expansions of approximately 2.4 nm with greater than seven-sigma confidence. This level of sensitivity is sufficient to distinguish membrane rearrangements proposed in stress-response and bleaching models. Importantly, the study demonstrates that such measurements are feasible *in vivo*, despite additional scattering contributions from host tissue.

Citation: Corkery, R. W., Garvey, C. J. & Houston, J. E. *In hospite* and *ex hospite* architecture of photosynthetic thylakoid membranes in *Symbiodinium* spp. using small-angle neutron scattering. *J. Appl. Cryst.* 58, 1516–1525 (2025). <https://doi.org/10.1107/S1600576725007332>

ESS Contact: Judith Houston

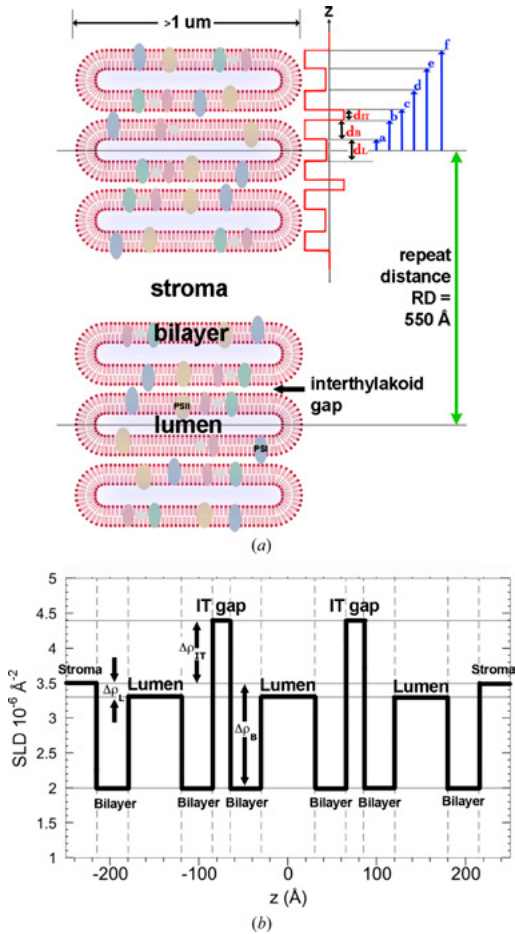


Figure 18. The triple-vesicle model for photosynthetic dinoflagellate thylakoid structures. Here $\Delta\rho_{IT}$, $\Delta\rho_B$, $\Delta\rho_L$ and d_{IT} , d_B , d_L are the SLD contrasts and thicknesses of the IT gap, bilayer and lumen, respectively. These are used in calculating the form factor of the triple-vesicle stack. Adjacent stacks are separated by a distance RD , which is used in the calculation of the structure factor. Coloured ovals in the lipid bilayers represent membrane proteins.



November

2025
HIGHLIGHTS

Following the structural changes of triolein films during lipolysis

This paper examines how lipase-catalysed lipolysis alters the internal structure of thin triolein films at a planar oil–water interface, with particular emphasis on the role of solution pD (the pH equivalent in D₂O). Understanding these structural changes is important because lipolysis is often self-limiting, restricting enzymatic efficiency in both biological and industrial contexts. The study focuses on *Thermomyces lanuginosus* lipase (TLL) acting on nanometre-scale triolein films at pD 7.0 and 8.5, chosen to lie on either side of the apparent pK_a of oleic acid.

Spectroscopic ellipsometry was used to follow changes in film thickness during lipolysis, while neutron reflectometry, including both specular and off-specular scattering, provided detailed insight into the internal film structure and its lateral heterogeneity. At pD 7.0, an initial lag phase is observed, followed by substantial thinning of the film as lipolysis proceeds. Neutron data reveal a buffer-equilibrated film containing large, water-filled conical protrusions penetrating the triolein layer, which are rapidly modified as lipolysis products accumulate at the interface. After digestion, the film reorganises into a perforated lipid layer with floating aggregates of hydrolysis products.

In contrast, at pD 8.5 the triolein film is significantly thicker and structurally more complex due to the presence of charged oleate species. Under these conditions, exposure to TLL produces little structural or thickness change, indicating strong inhibition of lipolysis, likely due to calcium oleate complexes or TRIS–oleate ion pairs forming an interfacial barrier.

Overall, the study demonstrates how pD controls both the kinetics and structural pathways of lipolysis and highlights neutron reflectometry as a powerful tool for resolving dynamic interfacial processes in lipid films.

Citation: Humphreys, B. A., Gutfreund, P., McCluskey, A. R., Arnold, T., Vind, J. & Nylander, T. Following the structural changes of triolein films during lipolysis. *Soft Matter* (2025). <https://doi.org/10.1039/d5sm00820d>

ESS Contact: Tom Arnold

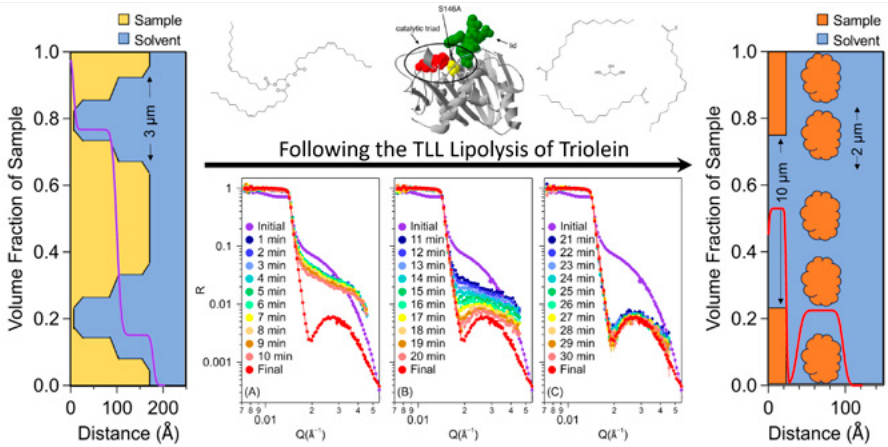


Figure 19. Structural evolution of thin triolein films during lipolysis, showing how the response depends strongly on solution pD. At pD 7.0, the film undergoes a lag phase followed by significant thinning and structural reorganisation, while at pD 8.5 it remains comparatively stable, indicating inhibition of enzymatic activity.



December | 2025 HIGHLIGHTS

Impact of extinction effects on neutron transmission in solid beryllium metal.

This paper investigates the impact of extinction effects on time-of-flight neutron transmission measurements in solid beryllium metal, with the aim of improving the accuracy of neutron cross-section data used in transport simulations and instrument design. Transmission and diffraction experiments were performed on four industrial beryllium grades using the HIPPO diffractometer at the Los Alamos Neutron Science Center, combining energy-resolved neutron imaging with simultaneous diffraction measurements.

The measured total neutron cross sections show a systematic reduction in the coherent elastic scattering component compared with predictions for an ideal polycrystalline material. Through detailed analysis, the authors demonstrate that this discrepancy cannot be explained by texture, absorption, impurities or Debye–Waller effects. Instead, it arises from extinction phenomena associated with dynamical diffraction within crystallites and grains. To model this behaviour, the Becker–Coppens extinction formalism was implemented within the NCrystal framework, allowing lattice-plane- and wavelength-dependent extinction corrections to be applied to the transmission data.

Fitting results show that secondary extinction dominates over primary extinction for all samples, although both contributions are required to achieve the best agreement with experiment. The extracted effective crystallite sizes are consistently smaller than the grain sizes measured by EBSD, consistent with sub-grain fragmentation caused by thermo-mechanical processing. Comparisons with historical cross-section measurements confirm that similar extinction effects were present but previously unaccounted for.

Overall, the study demonstrates that time-of-flight neutron transmission is highly sensitive to extinction effects and that these must be explicitly included in transmission analysis. The results provide a more physically realistic basis for modelling neutron interactions in beryllium components used at spallation neutron source.

Citation: Xu, S., DiJulio, D. D., Marquez Damian, J. I., Vogel, S. C., Long, A. M., Hirsh, T. Y., Kittelmann, T., Kuksenko, V. & Muhrer, G. Impact of extinction effects on neutron transmission in solid beryllium metal. *J. Appl. Cryst.* 58, 1957–1966 (2025). <https://doi.org/10.1107/S1600576725007939>

ESS Contact: Shuqi Xu, Douglas Di Julio, José Ignacio Marquez Damian, Thomas Kittelmann, Günter Muhrer

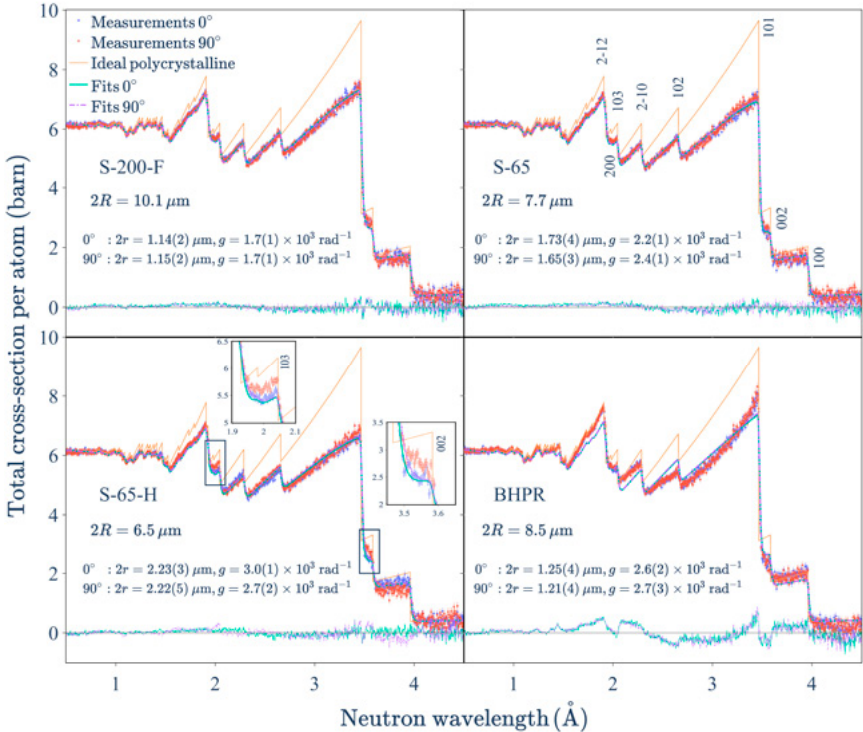


Figure 20. Neutron total cross sections of the beryllium grades S-200-F, S-65, S-65-H and BHPR, at two sample orientations 0° and 90° . Discrepancies are observed between the neutron transmission measurements and the cross sections based on the ideal polycrystalline assumption. The experimental data are interpreted using BC's extinction model through a least-squares fitting approach. The residuals of the fits are indicated along with the zero lines. The values of χ^2/ν are close to 2 for the S-200-F, S-65 and S-65-H grades but approximately 8 for the BHPR grade. Displayed values for $2R$ are the average grain sizes determined from the EBSD measurements.





Follow the ESS *Road to Science*

 @ess.neutron

 @essneutron

 @ESS-neutron

 @essneutron